



# Ethylene-vinyl acetate/poly (propylene carbonate) nanocomposites: effects of graphene oxide on microstructure, shape memory, and mechanical characteristics

Mohammad Javad Azizli<sup>1,2</sup> · Ehsan Vafa<sup>3</sup> · Somayeh Parham<sup>4</sup> · Katayoon Rezaeeparto<sup>4</sup> · Fatemeh Azizli<sup>5</sup> · Mohammad Hashemi<sup>2</sup> · Hesam Kamyab<sup>6,7,8</sup> · Shreshivadasan Chelliapan<sup>9</sup> · Ali Mohammad Amani<sup>3</sup> · Hengameh Honarkar<sup>10</sup> · Masoud Mokhtary<sup>1</sup>

Received: 26 December 2023 / Accepted: 25 April 2024 / Published online: 3 June 2024  
© The Polymer Society, Taipei 2024

## Abstract

The present study aims to introduce new shape memory composites containing different nanofillers including reduced graphene oxide nanoplatelets (rGONp), graphene oxide nanoplatelets (GONp), and their hybrids (rGONp/GONp) and based on ethylene-vinyl acetate copolymer, polypropylene-graft-maleic anhydride, and polypropylene carbonate (EVA/PP-g-MA/PPC). The morphologies of the synthesized nanocomposites were studied by transmission electron microscopy (TEM) and scanning electron microscopy (SEM), which showed that adding GO/rGO hybrid made better uniformity in the matrix rather than GO and rGO. Thermal gravimetric analysis (TGA) indicated that by adding nanofiller into the nanocomposites, the melting temperature ( $T_m$ ) increased from 68.7 °C to 70.9 °C, while the glass transition temperatures ( $T_g$ ) decreased from 33.1 °C to 30.6 °C. In addition, mechanical analysis illustrated that by adding nanofiller to the matrix, the breaking stress, modulus, and elongation-at-break increased about 321%, 193%, and 145%, respectively. Moreover, in the composites containing rGONp/GONp, the shape recovery and shape fixity enhanced in comparison with their rGONp and GONp counterparts. Therefore, the results revealed that the shape memory EVA/PP-g-MA/PPC mixture, including a hybrid of GONp and rGONp, has a high actuation value, superior mechanical strength, and excellent shape fixity. Finally, the obtained shape fixity of 98.7% and shape recovery of 95.9% for the synthesized samples are the best shape memory characteristics for the hybrid nanocomposites.

**Keywords** Shape memory · EVA/PP-g-MA/PPC · Nanocomposites · Morphology · Mechanical properties

✉ Mohammad Javad Azizli  
mohammadjavad.azizli@gmail.com

Ehsan Vafa  
Ehsanvafa1025@gmail.com

Ali Mohammad Amani  
amani\_a@sums.ac.ir

Hengameh Honarkar  
h.honarkar@ippi.ac.ir

<sup>1</sup> Department of Chemistry and Chemical Engineering, Rasht Branch, Islamic Azad University, Rasht, Iran

<sup>2</sup> SazePaidarElahie Company (Linkran Industrial Group), Tehran, Iran, P.O. Box: 1447813184

<sup>3</sup> Department of Medical Nanotechnology, School of Advanced Medical Sciences and Technologies, Shiraz University of Medical Sciences, Shiraz, Iran

<sup>4</sup> Research Institute of Petroleum Industry, P.O. Box: 14857-33111, Tehran, Iran

<sup>5</sup> Department of Computer Engineering, Shiraz Branch, Islamic Azad University, Shiraz, Iran

<sup>6</sup> Malaysia-Japan International Institute of Technology, Universiti Teknologi Malaysia, Jalan Sultan Yahya Petra, 54100 Kuala Lumpur, Malaysia

<sup>7</sup> Department of Biomaterials, Saveetha Dental College and Hospital, Saveetha Institute of Medical and Technical Sciences, Chennai 600 077, India

<sup>8</sup> Faculty of Architecture and Urbanism, UTE University, Calle Rumipamba S/N and Bourgeois, Quito, Ecuador

<sup>9</sup> Engineering Department, Razak Faculty of Technology & Informatics, Universiti Teknologi Malaysia, Jalan Sultan Yahya Petra, 54100 Kuala Lumpur, Malaysia

<sup>10</sup> Department of Polyurethane and Advanced Polymers, Iran Polymer and Petrochemical Institute, Tehran, Iran, P.O. Box 14975/112

## Introduction

The use of diverse materials such as polymers, ceramics, and nanocomposite is integral to life. It is used in medicine [1–4], bioengineering [5, 6], biomechanics [7, 8], aerospace [9], organic chemistry [10–12], and many other industries. However, in many cases, materials and instruments fail or are useless due to deformation or failure [13–15]. Therefore, the usage of polymer composites that cannot restore and recover themselves increases the cost in the mentioned industries. To face this challenge, shape-memory blends and polymer composites are among the best. Shape memory polymers are a group of smart polymeric materials that can return to their original and permanent state after creating a temporary state or changing shape [16, 17]. Shape-memory polymers can maintain two or three states, and the shape change between these states can be caused by temperature. Other stimuli that can cause such deformation are magnetic fields, electric fields, light, or solutions [18, 19]. Various parameters affect the memory of materials. The most important parameter that affects the shape memory polymers is the existence of the separate phases. The similarities in pristine components' structures lead to a higher degree of compatibility and result in better mechanical behaviors [20]. For instance, ethylene-vinyl acetate (EVA) incorporated with poly(propylene carbonate) (PPC) composites indicated good shape memory behavior with shape fixing and shape recovery ratios of about 90% [21]. In addition, adding additives to the shape memory composites as nanofiller, such as graphene oxide (GO), reduced graphene oxide (rGO), and their hybrids, increases the thermomechanical strength as well as shape memory, molecular interaction, and finer dispersion [22, 23]. Some research results have shown that the shape recovery speed can be increased with the help of nanofillers, which attributed to the uniform structure of the nanocomposite. Wang et al. produced a shape memory nanocomposite containing reduced graphene oxide (rGO) and showed that the recoverability of the composite is approximately 100%, taking only 5 s under 6 V [23]. In another study, Tan et al. prepared graphene oxide (GO)-filled shape memory polyurethane nanofibers and systematically investigated the morphological, thermal, and mechanical properties, surface wettability, and the shape memory effect. The results showed indicated that GO can be well dispersed within the shape memory composite matrix and that the introduction of GO significantly improves the mechanical strength, surface wettability, and thermal stability [24, 25]. The complex deformation and retrieval process in triple shape memory (TSM) is possible by remembering two temporary shapes and one permanent shape [26–28]. TSM materials are used in several

applications such as intelligent packaging, sensors, or biomedical devices, resulting in their unique properties such as low cost, lightweight, gentle response temperature, or biodegradability [29, 30]. One of the most interesting ways to achieve materials with a wide transition temperature or two separate transition temperatures is the use of block or graft copolymers or their blends [31–33]. The application of polymer blending is generally preferred to copolymerization because it is a more flexible and environmentally friendly method. Many TSM materials are manufactured from miscible polymer blends [34, 35]. However, unlike miscible blends, which show moderate properties, the properties of immiscible blends can exceed the properties of each component [36, 37]. In the method of using immiscible polymer blends, it is possible to control each component independently, so the manufacturing process will be very flexible [38]. Yang et al. studied TSM blends prepared by melt blending of ethylene- $\alpha$ -octene block copolymer (OBC), PCL (poly  $\epsilon$ -caprolactone), and poly(propylene carbonate) (PPC) [39, 40]. It was found that the TSM of the blend was influenced by the phase morphology. Ji and coworkers [41] reported the preparation of the film of an ethylene-vinyl acetate copolymer/polyurethane/poly(vinyl acetate) blend (EVA/PU/PVAc) by forced-assembly multilayer coextrusion. In addition, Jung and coworkers prepared a polyurethane/graphene nanocomposite using solution mixing [42]. The elastic modulus and tensile strength of the synthesized nanocomposite were outstanding, but its elongation at break was less than that of unmodified polyurethane. During another interesting research, by adding 1 wt% of functionalized graphene to the polyurethane [43, 44], the shape recovery percentage increased by 52%. In another work, Han and Chun [23] incorporated reduced graphene oxide and graphene oxide functionalized with diazonium salts into PU polymer. They showed that the functionalized nanocomposite has better shape memory properties than the nanocomposite reinforced with reduced graphene oxide, which could be ascribed to its finer dispersion and superior interaction. In the functionalized graphene oxide/PU nanocomposite, shape fixity ratio and shape recovery increased to 98% and 94%, respectively. The literature survey shows that several studies have been performed on the effect of two-dimensional carbonic platelets on TSM behavior. However, the effects of affinity and polarity of carbonic nanoplatelets on the dynamics of blend chains in the shape memory process throughout microphase-separated EVA/PP-g-MA/PPC nanocomposites have not been previously studied by other researchers.

In this study, the primary objective was to investigate the influence of graphene oxide on the microstructure, shape memory properties, and mechanical characteristics

of ethylene-vinyl acetate/poly (propylene carbonate) nanocomposites. The incorporation of graphene oxide was hypothesized to enhance the overall performance of the nanocomposites by improving their structural integrity and shape memory behavior. The composites were characterized by TEM and FE-SEM thermal stability, mechanical properties, XRD, and DMTA studied. By systematically analyzing the microstructure and mechanical properties of the nanocomposites with varying graphene oxide concentrations, this research aimed to provide valuable insights into the potential applications of these materials in advanced engineering and biomedical fields. Furthermore, the study sought to contribute to the ongoing efforts in developing innovative nanocomposite materials with superior properties for a wide range of practical applications.

## Materials and methods

### Materials

In this research, the ethylene-vinyl acetate copolymer (EVA) Ultra UL (00218CC3) grade was acquired from ExxonMobil Escorene™ Chemicals Company (United States of America, Houston, Texas). This particular grade had a vinyl acetate content of 18 weight%, a melting point index (at 190 degrees Celsius and 2.16 kg) of 1.7 g/10 minutes, and a density of 0.94 g per cubic centimeter. Polypropylene graft-maleic anhydride (PP-g-MA), which contains 1 weight% of maleic anhydride, poly (propylene carbonate), from the products of Sigma Aldrich, Berlin, Germany. Poly(propylene carbonate) (PPC), with specifications,  $M_w = 8.15 \times 10^5$  g/mol, from the products of Sigma Aldrich, Berlin, Germany. Benzoyl peroxide (BPO), acetone (analytical grade), and chloroform are all products that were purchased from Sigma Aldrich in Berlin, Germany for this study. For the synthesis of rGOnp and GOnp, the following materials were used: graphite, hydrazine hydrate, potassium permanganate ( $KMnO_4$ ), dimethylformamide (DMF), hydrogen peroxide ( $H_2O_2$ ), hydrochloric acid (HCl), and sulfuric acid ( $H_2SO_4$ ). All of these ingredients were purchased from Sigma Aldrich in Berlin, Germany.

### Preparation of nanocomposites

PPC and EVA were completely dried in a vacuum oven before use. Based on the formulation of a certain amount of EVA, PPC and PP-g-MA as well as rGOnp, GOnp and rGOnp/GOnp in a mixer (Haake) at a temperature of 95.0 °C and 20 r/min for 3 min, then 60 r/min for 10 minutes. The EVA/PP-g-MA/PPC blends were extruded and cut into pieces. The nanocomposites samples were subsequently compressed into 1 mm-thick 4 mm-width rectangular

samples at 100 °C and then treated under a pressure of 25 MPa at 125 °C for 20 min. Then the produced samples were slowly cooled in air.

### Thermal stability characterization

The thermal stability characterization of nanocomposites was performed in the temperature range of 100–800 °C, in a nitrogen gas environment with a heating rate of 5 °C/min, with a weighted thermal gravimetric analysis (TGA) model TGA4000 of PerkinElmer Company (USA). The samples with  $50 \pm 5$  mg were prepared to perform the analysis. To get reliable results and reduce possible errors, each sample was analyzed at least three times, and the average of their results was used in the calculations. Differential scanning calorimetry (DSC) measurements were performed on a TA Q2000 under a nitrogen atmosphere with a constant flow rate of 40 ml  $\text{min}^{-1}$ . Samples were dried in a vacuum oven. It was then heated from 0 °C to 100 °C at a heating rate of 20.0 °C/min. The procedure was conducted in three steps with approximately  $15 \pm 2$  mg of each sample: heating, cooling, and reheating. To get reliable results and reduce possible errors, each sample was analyzed at least three times and the average of their results was used in the calculations.

### Shape memory characterization

The shape memory behavior and thermo-mechanical decomposition of nanocomposites were investigated using a 500 TMA device manufactured by Polymer Laboratories (UK). To induce to induce the properties of shape memory, the sample was first heated to about  $T_g$  and kept at this temperature for 8 min. Then, about 1 MPa of stress was applied to the sample, and immediately the temperature of the sample was reduced to 12 °C with cold water with a temperature of 5 °C. At this temperature, the sample was kept under stress for 20 min. Finally, the stress was removed from the sample and then the temperature was increased to 45 °C. After that, strain changes against temperature, stress, and time were recorded. Changes in tablet thickness with temperature were calculated using a recorder device, and the values of reversibility ( $R_r$ ) and temporary shape stabilization ( $R_f$ ) were calculated from Eqs. 1 and 2:

$$R_f = \frac{\varepsilon_u}{\varepsilon_m} \quad (1)$$

$$R_r = \frac{\varepsilon_m - \varepsilon_p}{\varepsilon_m} \quad (2)$$

where  $\varepsilon_m$  is the maximum strain in the first stage,  $\varepsilon_u$  is the residual strain after cooling the sample and fixing its temporary shape, and  $\varepsilon_p$  is the recovered strain after reheating. To

get reliable results and reduce possible errors, each sample was analyzed at least five times and the average of the results was used in the calculations.

### XRD characterization

An X-ray diffractometer (X Pert MPD) was applied under a voltage and current of 40 kV and 40 mA, respectively,  $\lambda = 1.540 \text{ \AA}$ , using Cu K $\alpha$  radiation to investigate the fillers. For this test, the powder samples were put in the XRD pan where the room temperature was maintained. A hand-held Raman analyzer (First Guard model, Rigaku Co. USA) with a wavelength of 1064 nm in the spectral range of 500–2000  $\text{cm}^{-1}$  was used.

### Mechanical testing

Tensile tests were carried out according to ASTM D-412 standard method and with the help of the Zwick tensile machine (Germany) with a jaw speed of 500 mm/min at room temperature. To prepare the sample for the tensile test, a plate with a thickness of 2 mm was prepared at 160 °C with 180 bar, in a hydraulic hot press. The samples were cut in the form of dumbbells with specific features (2 × 25 × 120 mm) from plates. To get reliable results and reduce possible errors, each sample was analyzed at least five times and the average of the results was used in the calculations.

### Surface characterization

A transmission electron microscope (TEM, H9500 model, HITACHI Co, Japan) was used to study the distribution of nanofiller platelets in the polymer matrix. To prepare the samples, very thin films of the sample were prepared at refrigeration conditions of -75 °C using an ultra-microtome (Leica) equipped with a diamond knife, and then the surface was covered with gold layers. In addition, to examine the microstructure, the device (FE-SEM) model MIRA3 made by the TESCAN company was used at a voltage of 15 Kv and a resolution of 1.5 nm. After analysis, all of the samples were fractured in liquid nitrogen and their surfaces were coated with gold particles by using the chemical vapor deposition technique at a high vacuum.

### Dynamic mechanical thermal analysis (DMTA)

A Pyris Diamond DMTA device from Perkin Elmer Company (USA) was used to investigate the mechanical properties. This test was performed at a heating rate of 10 °C/min at a temperature range of -100 to 100 °C and at a frequency of 1 Hz and strain of 0.2% in the bending mode. For this purpose, the rectangular samples with dimensions of 16 × 5 × 50 mm were prepared. To get reliable results and

reduce possible errors, each sample was analyzed at least three times and the average of their results was used in the calculations. For the synthesis of rGOnp and GOnp, the Hummers method was used, the details of which can be found in references [45, 46]. A hydrazine hydrate-reducing agent was used for the chemical reduction of GOnp to synthesize rGOnp. Briefly, 0.2 kg of GOnp was poured into a 2000-mL round-bottomed flask and agitated magnetically to obtain an inhomogeneous dispersion with a yellow-brown color. An 85-watt ultrasonic bath was used, and the dispersion was sonicated for 150 minutes until a homogeneous GOnp dispersion was obtained. Then the reaction was continued by adding hydrazine hydrate for 48 hours at 80 °C in an oil bath with a water-cooled condenser fitted with the round-bottomed flask. The product was precipitated as a black precipitate and separated by vacuum filtration. To remove the unreacted hydrazine fully, the residue was washed several times with distilled ethanol and water. Lastly, a vacuum oven was used to dry the product at 35 °C for 48 hours. For this purpose, a pure suspension of rGOnp and GOnp and a hybrid of rGOnp/GOnp with the same ratio were used. For instance, 10 phr of hybrid rGOnp/GOnp (i.e., 5 phr rGOnp + 5 phr GOnp) was prepared in the DMF using ultrasonication (Hielscher 400 W) for 1 h. Thus, the use of ultrasound led to the breaking of large aggregates and the separation of rGOnp and GOnp. Before using the precursors, they were completely dried in an oven. To prepare the EVA/PP-g-MA/PPC (50:5:50) solution, a certain amount of EVA, PP-g-MA, and PPC was added in a mixer (HaakeRheomix 600) at a temperature of 95 °C and a speed of 10 r/min for 2 min, and mixing was continued at a speed of 50 r/min for another 6 min. After that, different amounts of nanofillers (0.1, 0.3, 0.5, 0.7, 1.0, and 1.3 phr of rGOnp, GOnp, and rGOnp/GOnp) were added to the mixture at 95 °C for 10 min at 50 r/min. The prepared samples were then compressed at 90 °C into rectangular pieces with a thickness of 1 mm and a width of 4 mm, and then treated at 120 °C for 25 min under a pressure of 10.0 MPa. Finally, the samples were slowly cooled in air and stored for further analysis. In coding blends, E stands for EVA, C stands for PP-g-MA compatibilizer, and P stands for PPC. GOnp stands for graphene oxide nanoplatelets; rGOnp stands for reduced graphene oxide nanoplatelets; and rGOnp/GOnp stands for a hybrid of rGOnp and GOnp.

## Results and discussion

### Evaluation of the nanofillers production

Figure 1a shows the XRD patterns of graphite nanofillers, rGOnp, and GOnp. As can be seen in this figure, changes in the distance between the interlayers of nanofiller structures

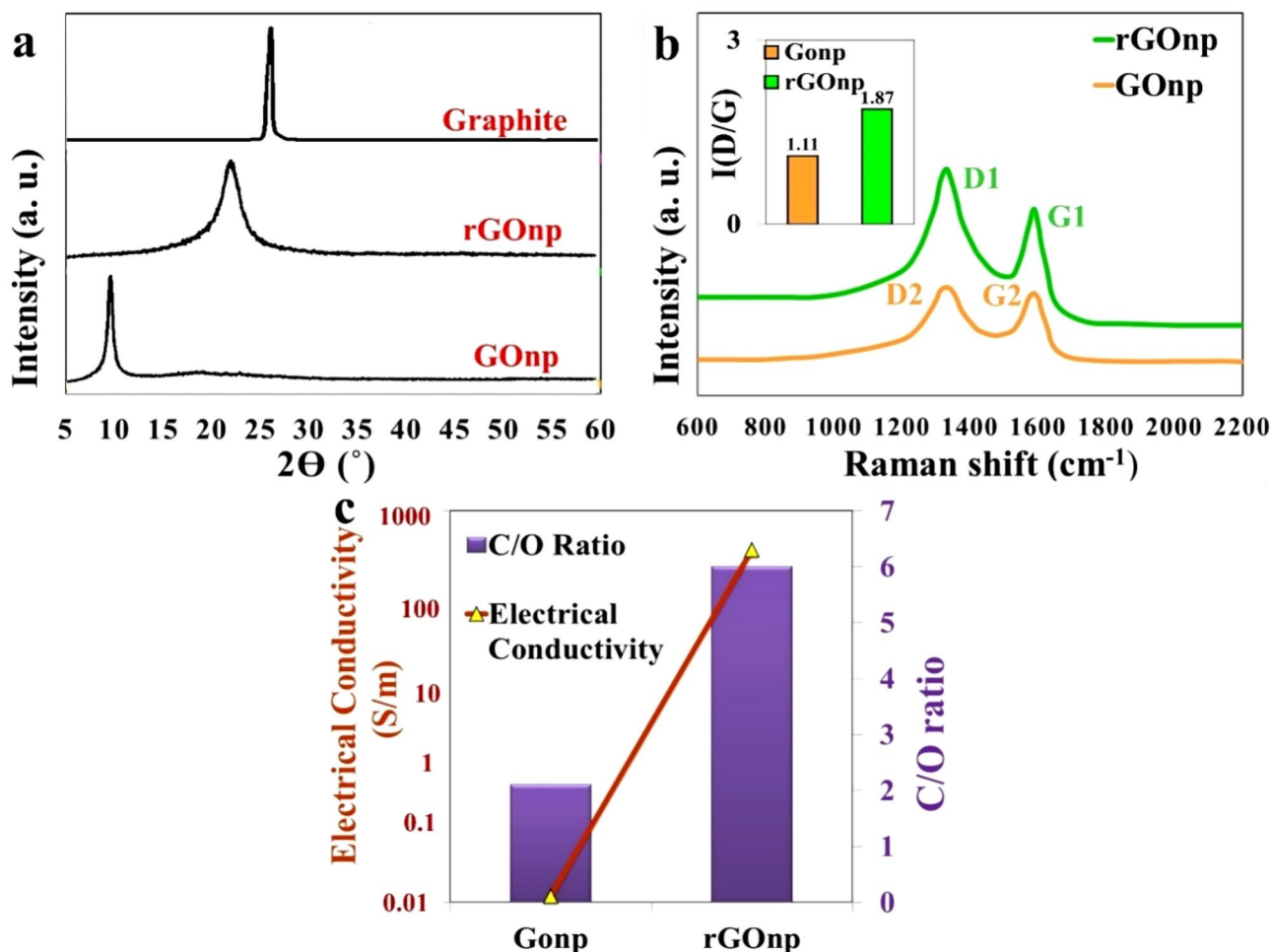


**Fig. 1** **a** XRD patterns of graphite, rGOnp and GOnp, **b** Raman spectroscopy results for rGOnp and GOnp, **c** Electrical conductivity and C/O ratio at  $10^3$  Hz for rGOnp and GOnp

can be investigated during the oxidation and reduction processes. The graphite characteristic peak is shifted from (002),  $2\theta = 25.7^\circ$  to (001),  $2\theta = 12.9^\circ$ , for GOnp. The presence of the oxygenated groups OH, -COOH, and epoxy increased the d-distance from approximately 0.33 nm for graphite to 1 nm for GOnp. These data are in good agreement with previously reported results [47, 48]. Furthermore, the characteristic peak of GOnp disappears due to the removal of oxygenated groups by the reduction process, but there are also small oxygen groups on the rGOnp surface arranged in a short range, leading to the appearance of a wide peak around (002),  $2\theta = 25.1^\circ$  reflection [49, 50]. The effect of carbanionic platelet functional groups on graphite d-spacing can be determined from experimental observations; consequently, rGOnp d-spacing is a little higher than graphite d-spacing (0.36 nm), suggesting the presence of structural flaws or some residual oxygenic groups [50]. Raman spectroscopy is a very special tool for examining disordered/ordered sp<sup>2</sup> structures. As can be seen in Fig. 1b,

the D (1350) and G (1600) peaks, and the Raman shift ( $\text{cm}^{-1}$ ) match the populations of SP<sup>2</sup> and SP<sup>3</sup> regions. Also, in this figure, the ratio of this peak (D to G) intensities (I(D/G)) clarified that the SP<sup>2</sup> structure population in nanofillers is higher than that in GOnp (I(D/G) rGOnp > I(D/G) GOnp). Therefore, by increasing the above ratio, the number of free electrons increases, which greatly affects the electrical conductivity of nanoparticles. The electrical conductivity of rGOnp and GOnp was measured to confirm that the removal of oxygenated groups can influence the conductivity of nanoparticles. As shown in Fig. 1c, the SP<sup>2</sup> structure of rGOnp and GOnp and their surface chemistry are affected by electrical conductivity and the ratio of C/O (carbon to oxygen) at 10<sup>3</sup> Hz. There is no doubt that the carbon-to-oxygen ratio for GOnp has increased from 2.01 to 5.98 for rGOnp, which can be attributed to the decrease in oxygen content in the reduction process. By converting GOnp into rGOnp, the electrical conductivity increases dramatically because the  $\pi$  bonds of rGOnp are stronger [44, 51], which is in agreement with the

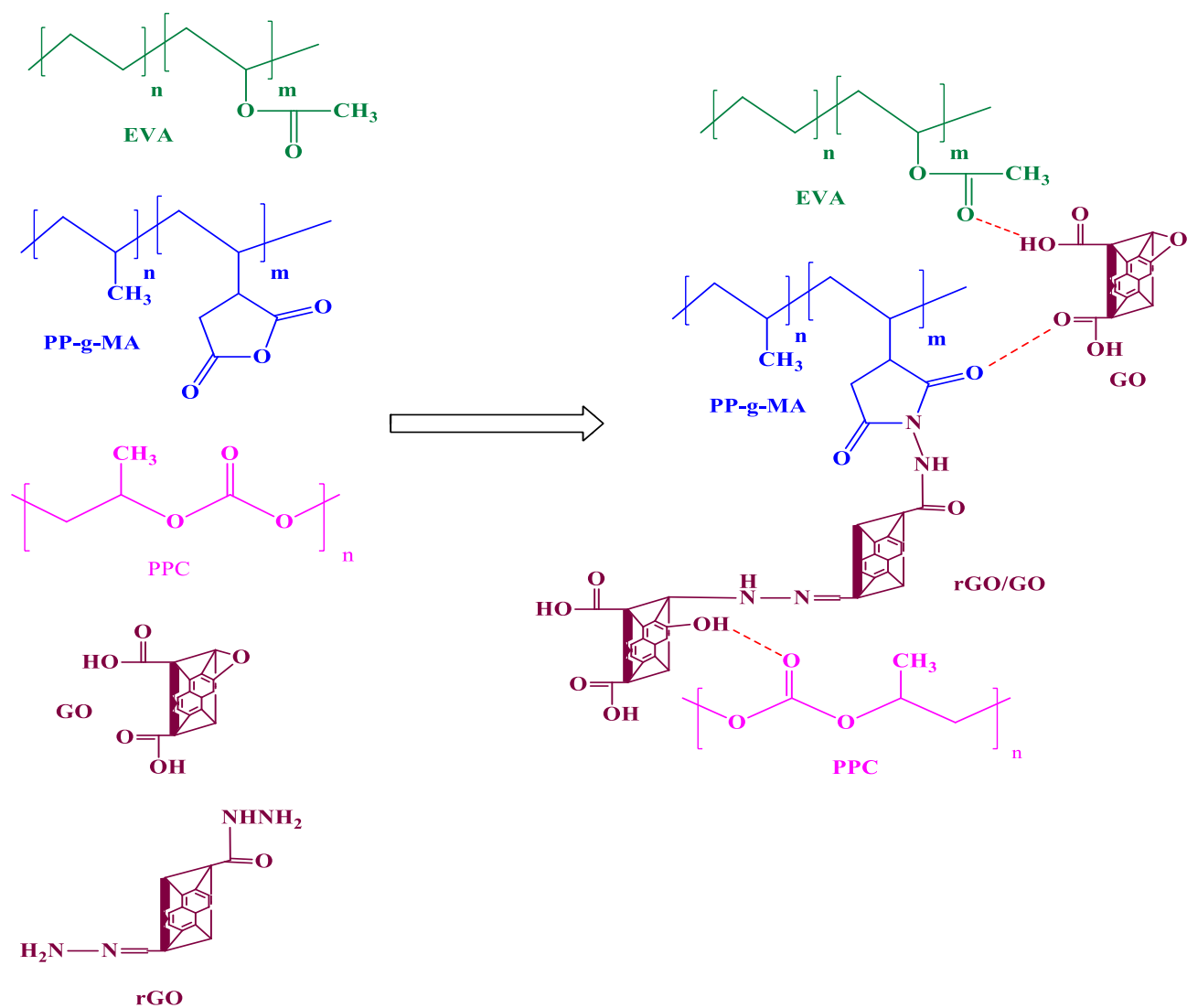


**Fig. 2** Possible interaction mechanism of EVA/PP-g-MA/PPC with rGOnp/GOnp

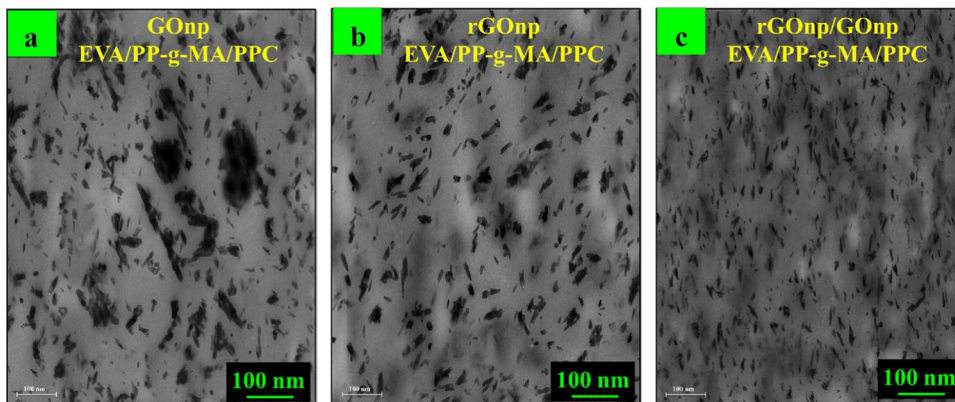
results of Raman spectroscopy. As shown in Fig. 2, a possible hydrogen bond interaction is formed between the carbonyl functional groups in EVA and PP-g-MA with the graphene oxide carboxyl functional group and the PPC carbonyl functional groups with the rGOnp/GOnp carboxyl functional group. According to the functional groups in PPC and EVA, there is no possibility of strong interaction between them. Adding rGOnp and GOnp causes hydrogen bond interaction between EVA/PP-g-MA and PPC (Fig. 2). This hydrogen bond interaction between composite components has made better compatibility between EVA and PPC.

### Morphological study

Figures 3 and 4 show the TEM and FE-SEM micrographs of EVA/PP-g-MA/PPC nanocomposites. The

microstructure of EVA/PP-g-MA/PPC/GOnp nanocomposites (Fig. 3a) demonstrates that nanofiller aggregates have an island/shape in the nanocomposites, which is due to the strong tendency between GOnp and the hard segments. Identifying EVA/PP-g-MA/PPC nanocomposites is a useful way to predict phase separation between soft and hard segments. The TEM image of rGOnp nanocomposites in Fig. 3b, shows that the rGOnp has good dispersion compared to GOnp which can be attributed to the migration of the nanofiller aggregates to soft segments continuing the phase of EVA/PP-g-MA/PPC. There is no doubt that different advantages and disadvantages can be found for the morphologies of EVA/PP-g-MA/PPC nanocomposites. In this way, the design of hybrid composites is possible through the simultaneous use of the same values of rGOnp and GOnp. Figure 3c shows the rGOnp/GOnp

**Fig. 3** TEM micrographs of EVA/PP-g-MA/PPC nanocomposites containing: **a** GOnp 1.3 phr, **b** rGOnp 1.3 phr, and **c** rGOnp/GOnp 1.3 phr



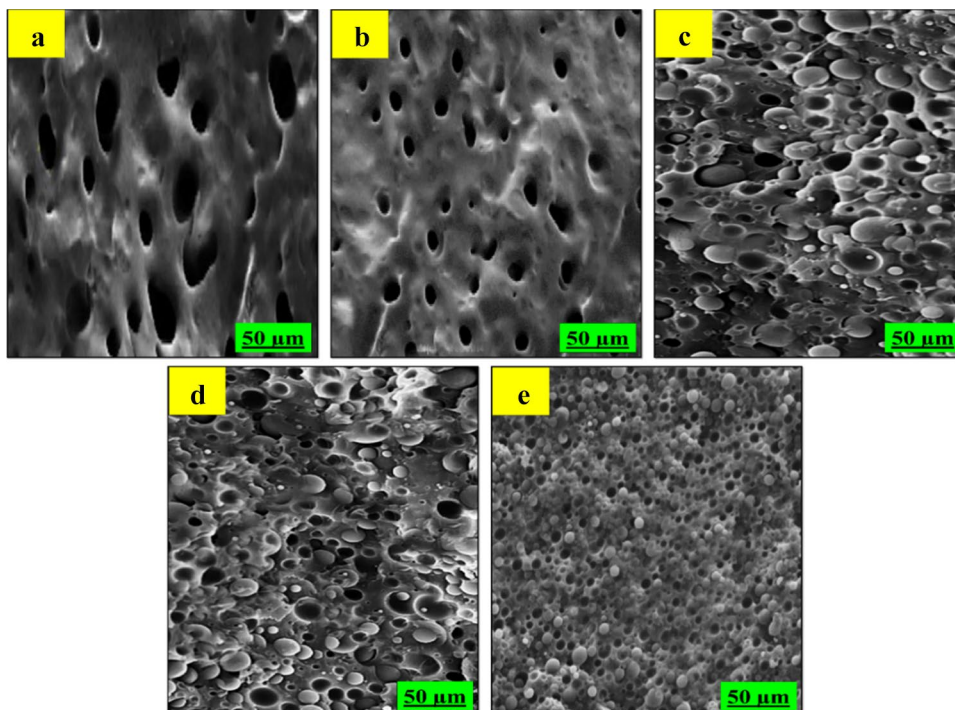
nanocomposites morphology. The dispersion of nanoparticles in hybrid nanocomposites containing 1.3 phrGOnp/GOnp is more homogeneous than the dispersion of nanoparticles in simple nanocomposites [52]. This is due to the hydrogen bonding between the carbonyl functional groups: EVA PP-g-MA with the carboxyl functional group of graphene oxide, and the PPC carbonyl functional groups with the rGOnp/GOnp carboxyl functional group (Fig. 1). The SEM micrographs of EVA/PPC containing PP-g-MA (b), GOnp (c), rGOnp (d), and rGOnp/GOnp (e) are presented in Fig. 4. As seen in this figure, the droplet size of the PPC polymer distributed in the EVA phase is reduced by the addition of rGOnp/GOnp, rGOnp, GOnp, and PP-g-MA, respectively. This is due to compatibility among EVA, PPC, and PP-g-MA (Fig. 4b), as well as compatibility of

EVA/PP-g-MA/PPC with rGOnp/GOnp, rGOnp and GOnp (Fig. 4c and e). The dispersion and droplet size of dispersed PPC as well as EVA/PP-g-MA/PPC compatibility are strongly influenced by nanofiller and PP-g-MA [53].

**Thermal properties**

It seems that the thermomechanical properties of EVA/PP-G-MA/PPC should be further studied because the thermal stability of hybrid EVA/PP-G-MA/PPC is severely affected by shape memory. Figure 5 shows the DSC curves of EVA/PP-g-MA/PPC nanocomposites containing various amounts of rGOnp, GOnp, and hybrid rGOnp/GOnp. The thermal characteristics of the hybrid EVA/PP-g-MA/PPC nanocomposites are presented in Table 1. Undeniably, the change

**Fig. 4** FE-SEM micrographs of EVA/PP-g-MA/PPC nanocomposites containing: **a** EVA/PPC blend, **b** EVA/PP-g-MA/PPC, **c** GOnp 1.3 phr, **d** rGOnp 1.3 phr. and **e** rGOnp/GOnp 1.3 phr

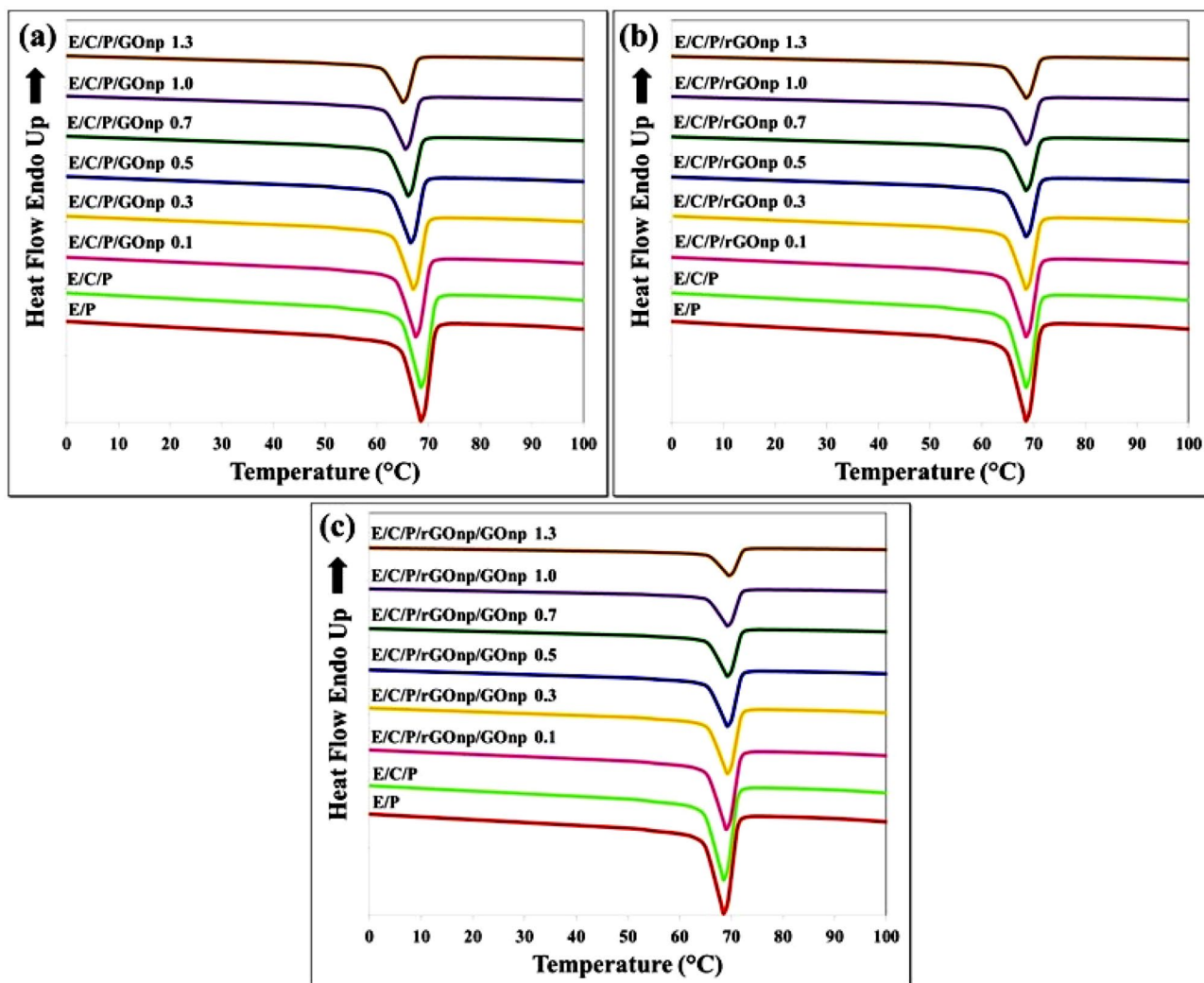


**Table 1** Thermal characteristics of EVA/PP-g-MA/PPC blends by increasing of rGOnp/GOnp

Sample	T <sub>m,h</sub> (°C)	T <sub>m,s</sub> (°C)	T <sub>g,s</sub> (°C)	X <sub>c</sub> (%)	ΔH (J/g)
E/P	155.6	68.7	33.1	13.3	24.3
E/C/P	155.8	68.9	33.3	13.6	25.1
E/C/P/GOnp/rGOnp 0.1	157.3	68.9	32.8	16.1	28.1
E/C/P/GOnp/rGOnp 0.3	158.2	69.5	32.4	16.9	28.3
E/C/P/GOnp/rGOnp 0.5	158.6	69.9	31.9	17.8	29.4
E/C/P/GOnp/rGOnp 0.7	158.9	70.2	31.5	18.8	29.8
E/C/P/GOnp/rGOnp 1.0	160.3	70.5	30.9	19.3	30.3
E/C/P/GOnp/rGOnp 1.3	160.8	70.9	30.6	19.9	30.1

in the glass transition temperature of soft segment (T<sub>g,s</sub>) of hybrid EVA/PP-g-MA/PPC nanocomposites is recognized, which is related to the physical ageing of the blends.

There is no doubt that a slight decrease in T<sub>g,s</sub> depends on an increase in GOnp (Table 1). The lower linkage fraction of EVA/PP-g-MA/PPC hybrid nanocomposites reduces the hydrogen bonding in the system, and therefore a strong interaction between GOnp and hard segments occurs [54]. In fact, it can be said that the interaction of GOnp with the hard segments in EVA/PP-g-MA/PPC hybrid nanocomposites increases the degree of freedom of soft segments, and consequently, the soft segments' melting point (T<sub>m,s</sub>) reduces in the presence of polar platelets. Actually, the GOnp localization in hard segments possibly will produce more microphase-separated morphology. It should be noted, however, that the effect of GOnp on the reduction of the mobility of the hard segment is severe, and this will increase the melting temperature of the hard segments (T<sub>m,h</sub>) as the GOnp content increases (Table 1). In addition, the presence of rGOnp reduces the movement of soft segments. By

**Fig. 5** DSC thermograms of EVA/PP-g-MA/PPC blends containing of: **a** GOnp, **b** rGOnp, and **c** hybrid rGOnp/GOnp (0.1, 0.3, 0.5, 0.7, 1.0 and 1.3 phr)



enhancing rGOnp, the  $T_{g,s}$  and  $T_{m,s}$  of hybrid EVA/PP-g-MA/PPC display a rising trend, but it does not have a strong effect on  $T_{m,h}$ . The results showed that rGOnp particles were located in the soft segments. As shown in Fig. 5 (DSC results) and Table 1, the soft segments of hybrid EVA/PP-g-MA/PPC can be crystallized, and rGOnp largely interacts with the soft segments, leading to their insignificant effect on  $T_{m,h}$ . The melting temperature of soft segments of EVA/PP-g-MA/PPC is 47.8 °C, which decreases with increasing rGOnp content. The following equation can be used to calculate the degree of crystallization ( $X_c$ ) of neat EVA/PPC and its nanocomposites:

$$X_c\% = \frac{\Delta H}{\Delta H_0} \times 100 \quad (3)$$

In this Eq,  $\Delta H$  and  $\Delta H_0$  represent the heat of fusion and the heat of fusion of 100% crystalline nanocomposites, respectively. The results are presented in Table 1. In terms of  $X_c$  and  $\Delta H$  values, it is comparatively obvious that the crystalline state value of hybrid EVA/PP-g-MA/PPC is increased, indicating the role of rGOnp as a nucleating agent in the soft segments. It should be noted that the higher the rGOnp, the higher the soft segment crystalline state of blends. In this way, the melting point will be higher, which is the result of the formation of more regular structures, or microcrystals. The phase-separated morphology of EVA/PP-g-MA/PPC further elucidated in the presence of rGOnp (low polarity) and GOnp (polarity), which can be explained based on the above descriptions and DSC observations. Although rGOnp is mainly located in the local soft segments, strong interactions between polar platelets and hard segments are confirmed only by the diversity of crystalline behavior. Overall, it can be concluded that rGOnp/EVA/PP-g-MA/PPC and GOnp/EVA/PP-g-MA/PPC nanocomposites have opposite two morphologies, each of which has its own advantages and disadvantages. A good effect on the crystallinity behavior in nanocomposites with non-polar platelets makes the shape memory behavior improved. Whereas the polar platelets make possible the development of shape memory properties with improved phase-separated

morphology in EVA/PP-g-MA/PPC nanocomposites. In hybrid rGOnp/GOnp of EVA/PP-g-MA/PPC nanocomposites, although the presence of GOnp is the reason for micro-phase separation, the tendency to increase the crystallinity of the composites is due to the nucleation effect of rGOnp. The data of hybrid nanocomposites in Table 1 showed that the  $T_{g,s}$ ,  $T_{m,s}$ ,  $X_c$ , and  $T_{m,h}$  values have increased with increasing rGOnp/GOnp content. In all these compounds, the abbreviation E stands for EVA polymer, the abbreviation C stands for PP-g-MA compatibilizer, and the abbreviation P stands for PPC polymer. Also, GOnp indicates the amount of graphene oxide nanoplatelets and rGOnp indicates the amount of reduced graphene oxide nanoplatelets and GOnp/rGOnp indicates a hybrid of both nanofillers in equal amounts. Also rGOnp/GOnp/EVA/PP-g-MA/PPC nanocomposites showed better improvement compared to both rGOnp/EVA/PP-g-MA/PPC and GOnp/EVA/PP-g-MA/PPC. The phase separation and crystallinity of rGOnp (pure) and GOnp at the same content are higher than those of rGOnp/GOnp hybrid. On rGOnp/GOnp/EVA/PP-g-MA/PPC nanocomposites, is expected to be more tunable, which leads to the creation of suitable features for the use of shape memory [55]. Supplementary data for Table 1 are available in the Supporting information (Table 1S).

### Mechanical properties of EVA/PP-g-MA/PPC nanocomposites

There is no doubt that by adding and incorporating rGOnp, GOnp, and rGOnp/GOnp hybrids into EVA/PP-g-MA/PPC blends, the mechanical properties are significantly increased [56, 57]. Many features are responsible for this increase in mechanical properties [58]. Nanofiller surface chemistry effects on the mechanical properties through nanofiller/nanofiller interaction, nanofiller/blend interaction, and nanofiller dispersion within the blend, which has been investigated in our study. Consequently, the different amounts (0.1, 0.3, 0.5, 0.7, 1.0, and 1.3 phr) of hybrid rGOnp/GOnp, rGOnp, and GOnp were incorporated into the EVA/PP-g-MA/PPC blends to study their influence on

**Table 2** Mechanical properties of EVA/PP-g-MA/PPC by increasing of rGOnp/GOnp

Sample	Youngs modulus (MPa)	Tensile strength-at-break (MPa)	Elongation-at-break (%)
E/P	3.61 ± 0.07	38.8 ± 0.76	55.9 ± 1.2
E/C/P	3.63 ± 0.07	40.3 ± 0.80	59.8 ± 1.2
E/C/P/GOnp/rGOnp 0.1	7.16 ± 0.14	57.1 ± 1.1	66.8 ± 1.3
E/C/P/GOnp/rGOnp 0.3	8.41 ± 0.16	61.4 ± 1.2	71.5 ± 1.4
E/C/P/GOnp/rGOnp 0.5	9.53 ± 0.18	68.2 ± 1.4	76.3 ± 1.5
E/C/P/GOnp/rGOnp 0.7	10.46 ± 0.21	71.4 ± 1.4	79.4 ± 1.6
E/C/P/GOnp/rGOnp 1.0	11.58 ± 0.23	74.7 ± 1.5	81.3 ± 1.6
E/C/P/GOnp/rGOnp 1.3	11.62 ± 0.23	74.9 ± 1.5	81.5 ± 1.6

the tensile strength, Young's modulus, and elongation-at-break of nanocomposites. As seen in Table 2, it is obvious that the mechanical properties of all EVA/PP-g-MA/PPC nanocomposites are higher than those of the EVA/PPC composites, and that the properties change with nano filler content. Table 2 shows that the tensile strength and Young's modulus at the breakpoint of the EVA/PP-g-MA/PPC/GO nanocomposite are greater than those of EVA/PPC blend. All of the mechanical properties are enhanced up to 1.3 phr GOnp, and the elongation-at-break to 1.3 phr GOnp is enhanced over that of other EVA/PPC blends due to enhanced nanofiller/nanofiller interaction. The Young's modulus values are enhanced from 3.61 MPa for the EVA/PPC blend to 9.89 MPa for 1.3 phr of EVA/PP-g-MA/PPC nanocomposites. Strain hardening causes a sharp increase in tensile strength at the breaking point of the EVA/PP-g-MA/PPC nanocomposites, which is simplified by increasing the hybrid rGOnp/GOnp, rGOnp, and GOnp content. The existence of covalent hydrogen bonding between carbonyl functional groups in EVA, PP-g-MA with carboxyl functional group of graphene oxide, and PPC carbonyl functional groups with rGOnp/GOnp carboxyl functional group in the hard segment of EVA/PP-g-MA/PPC nanocomposites plays an important role in the increased mechanical behavior. It is due the load transfer from EVA/PP-g-MA/PPC nanocomposites to the GOnp. It is found that elongation at break, tensile strength, and Young's modulus are improved by the addition of rGOnp to EVA/PP-g-MA/PPC blends at the same nanofiller content. Increasing the rGOnp content from phr 0.1 phr to 1.3 phr reduced the elongation-at-break from 65.9 to 62.8%. This decrease in elongation is due to the formation of the rGOnp network in EVA/PP-g-MA/PPC nanocomposites. However, it should be noted that the distribution of this network in the continuous/soft segment is an important reason that makes the network completion require less nanofiller. For rGOnp nanofiller nanocomposites, increasing the content of nanofiller leads to an increase in Young's modulus and strength-at-break. As can be seen in Table 2, the effect of adding rGOnp on enhancing the properties of EVA/PP-g-MA/PPC is far greater than that of GOnp. The reason for this discrepancy may be related to the following two factors. The first is the effect of plasticization and increasing the free volume of GOnp, which will be discussed in detail below. When the sample is subjected to a tensile load, the amount of movement in soft segments is greater than that in hard segments, so the continuous phase causes the chain to move when stress is loaded. The second reason is the presence of rGOnp in the vicinity of the soft segment of EVA/PP-g-MA/PPC nanocomposite chains. Table 2 shows the results of EVA/PP-g-MA/PPC nanocomposites containing hybrid rGOnp/GOnp. Supplementary data for Table 2 are available in the Supporting information (Table 2S). The increase in elongation at break, tensile strength, and Young's

modulus in nanocomposites containing hybrid nanofillers has more positive changes with the increase of nanofillers compared to nanocomposites containing simple nanofillers. It has already been stated that GOnp and rGOnp are attached to the soft and hard segments of the EVA/PP-g-MA/PPC chain, respectively, and that the reinforcing mechanism of each is unique. The rGOnp/GOnp hybrid showed the highest mechanical properties due to the synergistic effect between the two nanofillers. The addition of hybrid rGOnp/GOnp to EVA/PP-g-MA/PPC nanocomposites increased the modulus from 7.16 for 0.1 phr of rGOnp/GOnp to 11.62 for 1.3 phr of rGOnp/GOnp. Accordingly, the existence of rGOnp near GOnp increases the mechanical properties without compromising the high strain at break, however, the increase in elongation at break in simple blends is due to the sliding of GOnp and rGOnp layers on each other in hybrid composites. In fact, in hybrid composites, the benefits of each of the GOnp and rGOnp nanoparticles are retained. At the same nanoparticle content, a nanocomposite containing a rGOnp/GOnp hybrid has more flexibility than nanocomposites containing rGOnp and GOnp. Hence, hybrid rGOnp/GOnp nanocomposites have greater mechanical properties compared to rGOnp and GOnp nanocomposites [59].

### DMTA properties

Dynamic-mechanical thermal analysis (DMTA) is one of the most powerful tools for evaluating the dynamics of polymer chains in the presence and absence of nanofillers. The loss factor ( $\tan\delta$ ) and storage modulus of the neat EVA/PPC blend and its nanocomposites are shown in Fig. 6. For the sample without PP-g-MA compatibilizer (EVA/PPC), two separate peaks were observed at  $-34^\circ\text{C}$  and  $38^\circ\text{C}$  for EVA and PPC, respectively. However, with the addition of PP-g-MA, a peak was seen, which is probably due to the compatibility between the two incompatible polymers, EVA and PPC. The main reason for improving the EVA/PP-g-MA/PPC nanocomposites by reducing temperature is reducing the mobility of polymer chain segments in the glassy region. As can be observed in Fig. 6, the storage modulus of EVA/PP-g-MA/PPC/GOnp nanocomposites is higher than that of EVA/PPC blend and EVA/PP-g-MA/PPC. In fact, the presence of hydrogen bonding between the hard segments and the GOnp polar groups prevents the chains in the glass region from moving. A similar reason can be considered for increasing the storage modulus in the rubber region ( $25^\circ\text{C}$ ) from 5.79 MPa for EVA/PPC blend and 5.93 MPa for EVA/PP-g-MA/PPC to 6.43, 6.81, 7.25, 7.45, 7.68, 7.83 and 7.99 MPa for EVA/PP-g-MA/PPC/GOnp composite containing 0.1, 0.3, 0.5, 0.7, 1 and 1.3 phr GOnp, respectively. Table 3 shows the changes in the storage modulus in both the rubbery and glassy regions. Noticeably, the integral of  $\tan\delta$  peak for all composites is less than that of the EVA/

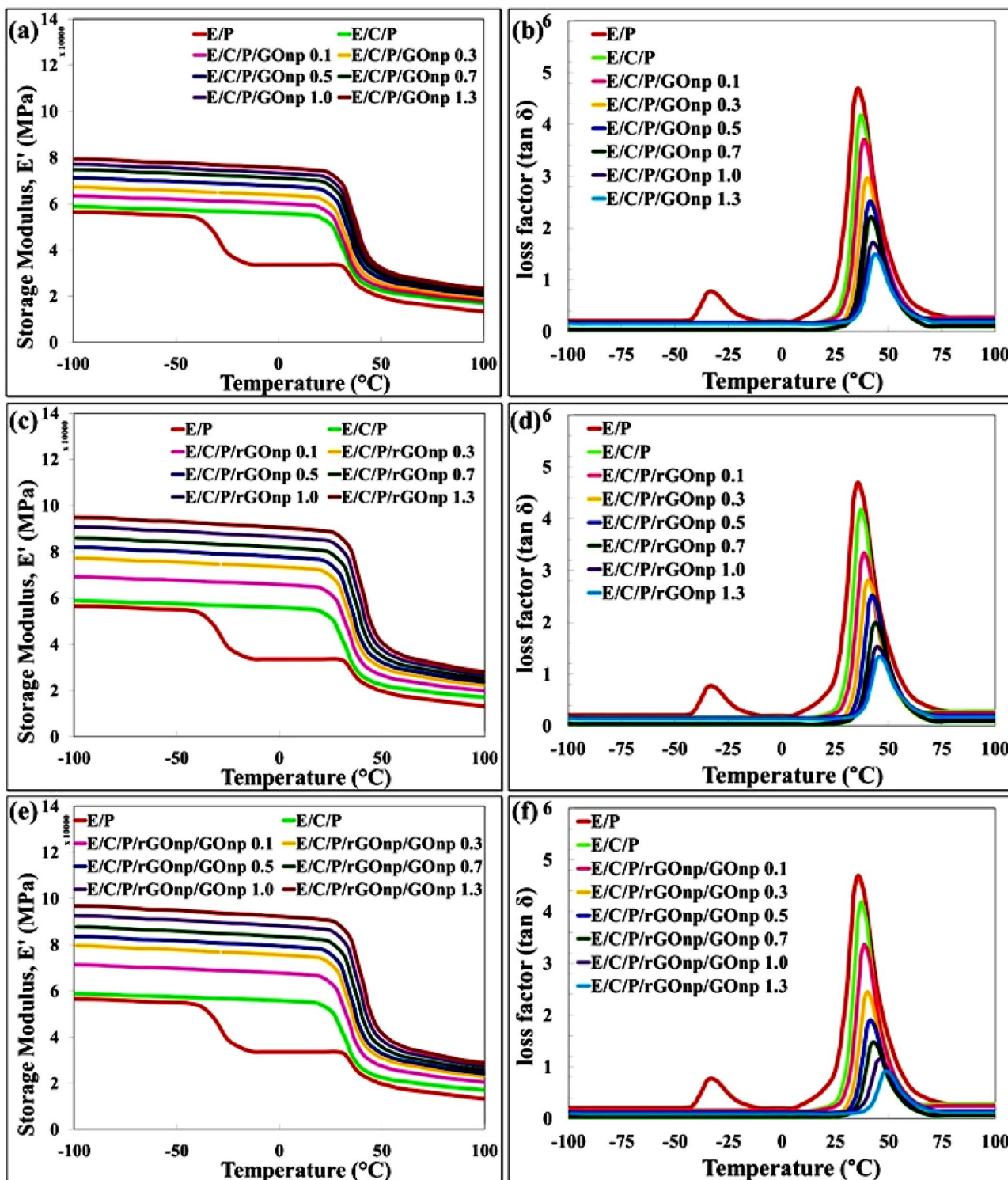


Fig. 6 DMTA curves of EVA/PP-g-MA/PPC nanocomposites containing GOnp, rGOnp, and hybrid rGOnp/GOnp (0.1, 0.3, 0.5, 0.7, 1.0 and 1.3 phr)

PPC blend. This indicates the correct interaction between the nanofiller and the polymer in the interfacial zone (Fig. 6b, d, and f). In fact, it can be said that in all nanocomposites, with increasing the content of rGOnp and GOnp, the storage

modulus increases, which is more in rGOnp nanocomposites than in GOnp nanocomposites (Table 3; Fig. 6c). This is due to the strong interaction between the soft segments and rGOnp. At room temperature, soft segments are in a

**Table 3** DMTA data of EVA/PP-g-MA/PPC nanocomposites containing hybrid rGOnp/GOnp (0.1, 0.3, 0.5, 0.7, 1.0 and 1.3 phr)

Samples	T <sub>g</sub> from E'' [°C]	T <sub>g</sub> from tan δ [°C]	Height of T <sub>g</sub> peak [-]	Decrease in peak tan δ [-]	E' at 25 °C [MPa]
E/P	-33.67 ± 0.67	-31.96 ± 0.63	0.92 ± 0.01	0	5.91 ± 0.11
E/C/P	38.96 ± 0.77	36.88 ± 0.73	4.98 ± 0.09	0	5.97 ± 0.11
E/C/P/rGOnp/GOnp 0.1	40.15 ± 0.80	49.82 ± 0.99	4.66 ± 0.09	0.32 ± 0.00	7.21 ± 0.14
E/C/P/rGOnp/GOnp 0.3	44.06 ± 0.88	42.88 ± 0.85	3.81 ± 0.07	1.17 ± 0.02	8.02 ± 0.16
E/C/P/rGOnp/GOnp 0.5	45.08 ± 0.90	43.91 ± 0.87	2.86 ± 0.05	2.12 ± 0.04	8.33 ± 0.16
E/C/P/rGOnp/GOnp 0.7	46.12 ± 0.92	44.89 ± 0.89	2.43 ± 0.04	2.55 ± 0.05	8.65 ± 0.17
E/C/P/rGOnp/GOnp 1.0	47.02 ± 0.94	45.53 ± 0.91	2.11 ± 0.04	2.87 ± 0.06	9.36 ± 0.18
E/C/P/rGOnp/GOnp 1.3	48.16 ± 0.96	46.77 ± 0.93	1.79 ± 0.03	3.19 ± 0.06	9.66 ± 0.19
E/C/P/rGOnp/GOnp 1.3	49.01 ± 0.98	47.86 ± 0.95	1.58 ± 0.03	3.40 ± 0.06	9.66 ± 0.19

rubbery state and have high flexibility compared to hard segments due to their high entropy. It must be said that at the same nanofiller loading, the storage modulus of EVA/PP-g-MA/PPC/GOnp nanocomposites is lower than that of EVA/PP-g-MA/PPC/rGOnp nanocomposites in the glassy and rubbery regions, because GOnp and rGOnp particles are located in the hard and soft segments, respectively. The tanδ curves of EVA/PP-g-MA/PPC nanocomposites comprising GOnp and rGOnp are illustrated in Fig. 6b and d, respectively. The maximum peak tanδ represents T<sub>g,s</sub> (glass transition of soft segments), and the related data for GOnp and rGOnp nanocomposites are listed in Table 3. By adding GOnp to EVA/PPC blends, the T<sub>g,s</sub> increased from -34.2 °C for EVA and 38.1 °C for PPC, and 38.3 °C for EVA/PP-g-MA/PPC to 38.6, 39.2, 40.3, 41.1, 41.9, 42.8, and 43.6 °C for EVA/PP-g-MA/PPC/GOnp nanocomposites comprising 0.1, 0.3, 0.5, 0.7, 1, and 1.3 phr GOnp, respectively. On the other hand, since rGOnp is located in soft segments, T<sub>g,s</sub> increases with increasing rGOnp content in the EVA/PP-g-MA/PPC blend. These results confirm the DSC tests and prove that in the presence of GOnp, the free volume of the soft segments is larger. As mentioned in the previous sections, here DMTA confirms the synergistic effect of the presence of two nanofillers in the nanocomposites. Thus, by limiting the movement of soft and hard segments that result from this phenomenon, the storage modulus in hybrid composites increases incredibly. For example, the storage modulus of EVA/PP-g-MA/PPC containing 1.3 phr hybrid rGOnp/GOnp is 9.8 MPa for the glassy state and 5.8 MPa for the rubbery state, which is absolutely greater than that of the EVA/PPC blend containing rGOnp and GOnp (1.3 phr). Nevertheless, the more intense storage modulus is offered in hybrid composites, but the dissipation mechanisms are exactly controlled because of the plasticizing effect of GOnp and the reinforcing effect on rGOnp at the soft segment of EVA/PP-g-MA/PPC, simultaneously. Previous descriptions can be confirmed using the T<sub>g,s</sub> data of EVA/PP-g-MA/PPC nanocomposites containing hybrid rGOnp/GOnp

presented in Table 3. At the same nanofiller content, the order of T<sub>g,s</sub> for nanocomposites containing nanofillers is as follows: rGOnp > rGOnp/GOnp > GOnp. As the rGOnp/GOnp hybrid increases, the dissipation mechanics undergo a uniform upward trend due to the increase in the interfacial zone. However, it is interesting to note that the difference in the glass temperature measured by thermal and mechanical methods lies in their work basis, in fact, the first is based on changes in heat capacity and the second is based on the mechanical response of polymer chain segments [60].

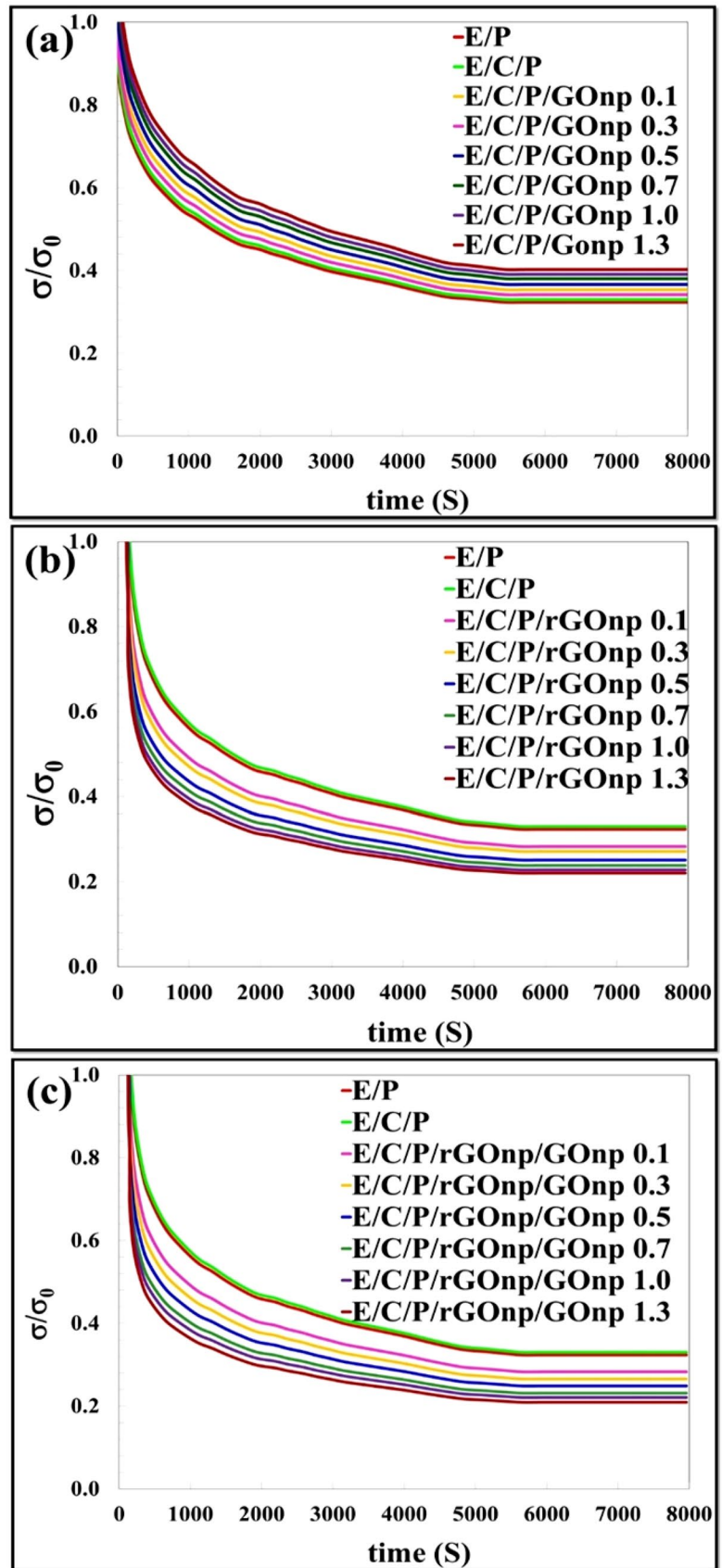
### Stress relaxation measurement

It has been shown that by measuring stress relaxation, a more complete understanding of the presence of rGOnp and GOnp in the dynamics of soft segments can be obtained. When a substance is exposed to a stress relaxation process in which two contrasting parts are recognizable: one part is the elastic part that stores energy in the material and the other part is the viscous part, which causes energy loss in the material by irreversible deformation of the chains. Thus, the more stress is reduced, the more permanent the deformation of the material [61]. Figure 7 shows the stress relaxation curves for EVA/PP-g-MA/PPC nanocomposites containing 0.1, 0.3, 0.5, 0.7, 1, and 1.3 phr of rGOnp, GOnp, and hybrid rGOnp/GOnp at a constant elongation of 70% at 25 °C. The famous Kohlrausch equation was used to calculate the relaxation time (τ) to fit the experimental results of the nanocomposite [62].

$$\frac{\sigma}{\sigma_0} = \frac{\sigma_\infty}{\sigma_0} + \frac{A}{\sigma_0} \exp\left[-\left(\frac{t}{\tau}\right)^\beta\right] \quad (4)$$

In this equation, β, σ<sub>∞</sub>, σ<sub>0</sub>, A, σ and t are the fitting parameters, remaining stress after infinitely long times, initial stress, fitting parameters, and stress during the time and time, respectively. Since this test is performed at high T<sub>g,s</sub>, it is necessary that the relaxation time be by the dynamic of

**Fig. 7** Stress relaxation curves for EVA/PP-g-MA/PPC nanocomposites containing: **a** GOnp, **b** rGOnp, and **c** hybrid rGOnp/GOnp (0.1, 0.3, 0.5, 0.7, 1.0 and 1.3 phr)



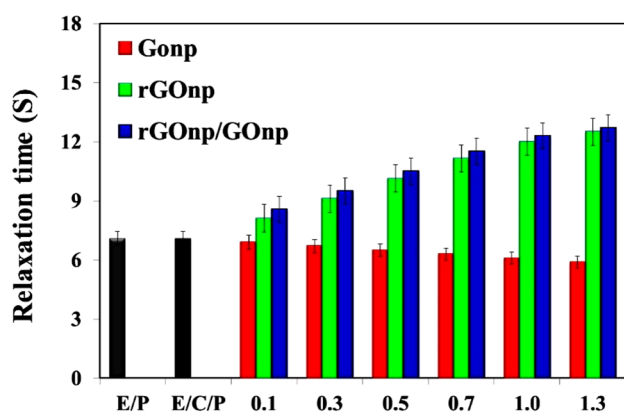


**Fig. 8** Relaxation time of EVA/PP-g-MA/PPC nanocomposites containing GOnp, rGOnp, and hybrid rGOnp/GOnp (0.1, 0.3, 0.5, 0.7, 1.0 and 1.3 phr)

the soft segment. Figure 8a shows the relaxation results for GOnp nanocomposites. According to this figure, the fast relaxation behavior under stress for the EVA/PPC and EVA/PP-g-MA/PPC blends in this nanocomposite is observed. GOnp has been shown to increase free volume, and of course, rearrangement, movement, and chain orientation are responsible for this phenomenon. The fit between the theoretical and experimental values is acceptable, and Fig. 9 shows the calculated relaxation times. EVA/PPC, EVA/PP-g-MA/PPC, EVA/PP-g-MA/PPC/0.1, 0.3, 0.5, 0.7, 1, and 1.3 phr GOnp nanocomposites have relaxation times of 6.3, 6.2, 5.8, 5.3, 5.1, 4.8, 4.6, and 4.5 s, respectively, whereas the relaxation time of the nanofiller/free sample is greater than that of GOnp nanocomposites (7.1 s) [62]. It was found that the higher the amount of GOnp in the composite, the greater the free volume in the soft segments. Indeed, the relaxation share for rGOnp nanocomposites is greater than that for EVA/PPC blends and EVA/PP-g-MA/PPC (Fig. 7b). Figure 7(a–c). It should be noted that the increase in rGOnp content decreased the soft segment dynamics in EVA/PP-g-MA/PPC/rGOnp. Since the concentration of rGOnp is high, the chemical reactions and physical interactions between the soft segments and rGOnp will be very high, and therefore such a decrease will be observed. The above descriptions can be confirmed by evaluating the EVA/PP-g-MA/PPC/rGOnp relaxation times. The high engagement between rGOnp and the soft segments at the interfacial region has caused the relaxation time for 1.3 phr this nanoparticle to reach its highest value of ~11.4 s. By adding GOnp, the stress-relaxation process slows down as the number of hard segments is reduced, so the flexibility and increase in the length of the chain will increase and we will see a change in the microphase separation degree. In addition, the reduction in the slow stress relaxation process and the overall flexibility of the chain confirms the localization of rGOnp in the

soft segment of the EVA/PP-g-MA/PPC nanocomposites. As seen in Fig. 8, the relaxation curves for hybrid rGOnp/GOnp nanocomposites and rGOnp nanocomposites are the same. The reason for this can be attributed to the interactions between rGOnp and soft segments, which again can be attributed to the creation of free volume through the presence of GOnp. As expected, the hybrid rGOnp/GOnp nanocomposites show greater and lesser relaxation times than GOnp and rGOnp nanocomposites at comparable nanofiller contents. Similarly, Fig. 8 shows that the relaxation time regularly increases from 8.2 s at 0.1 phr to 14.4 s at 1.3 phr for hybrid rGOnp/GOnp [61, 63].

### Shape memory properties

The shape memory properties, including shape fixity and shape recovery, of EVA/PPC and rGOnp, GOnp, and hybrid rGOnp/GOnp nanocomposites were investigated by thermomechanical analysis, and their results are presented in Fig. 9. Figure 9a shows the changes in temperature, strain, and stress over time during shape memory programming for the EVA/PPC blend. It is well established that shape memory behavior is the ability of a polymer to temporarily maintain its shape over the long term. According to Fig. 9b, it can be concluded that the shape memory properties in polymer systems are due to the effects of two phases. An unstable phase is related to the transition temperatures of soft segments in the EVA/PPC blend ( $T_{g,s}$ ), and a crystalline phase (physical net points) that has a fixed role in the EVA/PPC blend and is often related to hard segments. By heating the EVA/PPC blend and EVA/PP-g-MA/PPC nanocomposites close to  $T_g$ , a reversible phase transition was observed. For the sample to release stress and the frozen soft chains to return to their original random conformation, it is necessary to apply a stimulus field (heat) in the frozen state. In the meantime, fixity and shape recovery are ascribed to the free volume, crystallinity of soft segments, physical and chemical interactions, and dynamics in polymer composites. The hard and soft segments in the polymer composites are related to the transition between the reversible and the fixed phases. As Fig. 10 shows, the presence of GOnp has a strong effect on the shape stability of the EVA/PPC blend. With increasing the GOnp content from 0 to 1.3 phr, the shape fixity percentage increased from 93.8% for the EVA/PPC blend to 99.1% for EVA/PP-g-MA/PPC/GOnp due to an increase in the crystalline state. Contradictory findings have been reported for the shape fixity values of nanocomposites. In EVA/PP-g-MA/PPC/rGOnp nanocomposites, with increasing rGOnp content, a slight decrease is observed uniformly in the shape fixity values. Since rGOnp is present in the soft phase and causes even weaker programming in the EVA/PPC blend, there

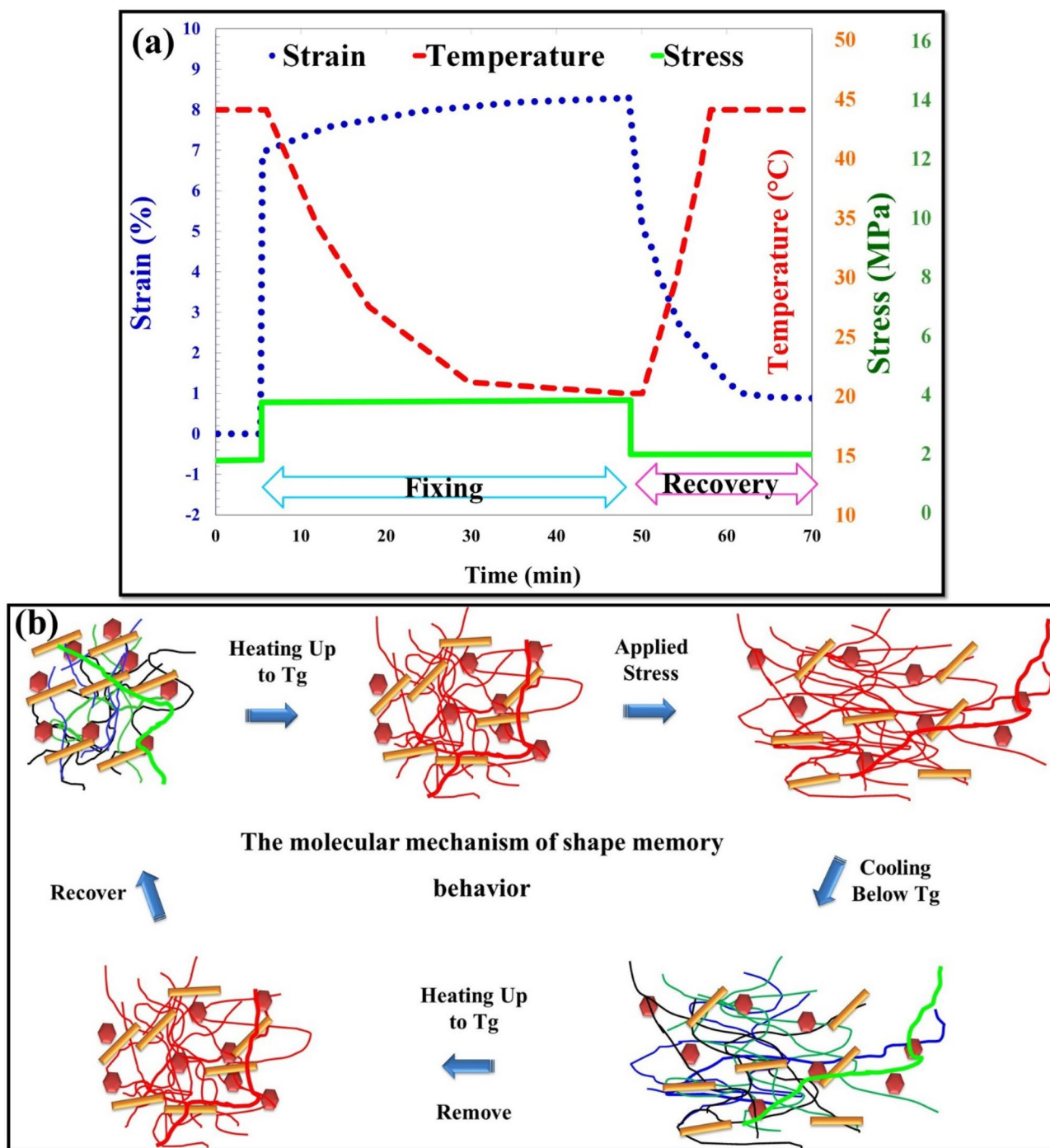
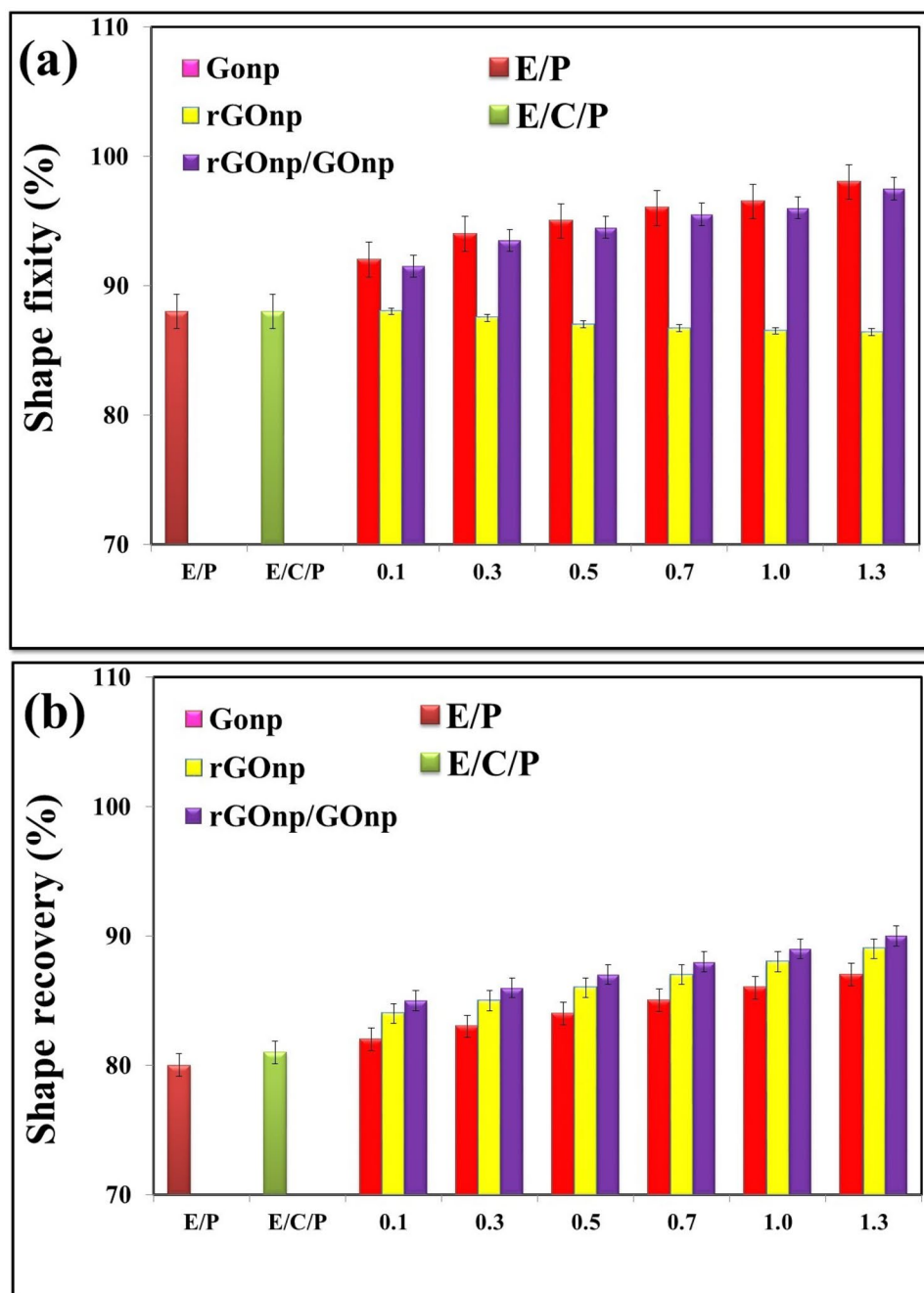


**Fig. 9** a Shape memory behavior: strain-temperature, stress-temperature, and time-temperature changes, b Schematic of possible shape memory mechanism of EVA/PP-g-MA/PPC blend

is no doubt that the difference in the shape fixity value is primarily due to the chain mobility of the soft parts under the programming process. In this research work, the lower the GOnp content, the higher the interfacial region and the interaction between the nanofiller and the polymer, and therefore the shape fixity decreased. In the following, you

will see how the introduction of the rGOnp/GOnp hybrid nanofiller increased the shape fixity of hybrid nanocomposites. As rGOnp/GOnp content increased, the shape fixity value increased uniformly until it reached its best value of 99.4 at 1.3 phr. This can be attributed to the dynamics of the optimal chains in the simultaneous presence of rGOnp

**Fig. 10** **a** shape fixity, and **b** shape recovery of EVA/PP-g-MA/PPC nanocomposites containing GOnp, rGOnp, and hybrid rGOnp/GOnp (0.1, 0.3, 0.5, 0.7, 1.0 and 1.3 phr)



and GOnp because each nanofiller can play its role. The shape recovery of EVA/PP-g-MA/PPC nanocomposites showed an outstanding enhancement with the incorporation of hybrid rGOnp/GOnp, rGOnp, and GOnp, as can be seen in Fig. 10b. As mentioned earlier, shape memory polymer composites must have a reversible phase (soft) and a fixed rigid phase (hard segments), so it is necessary to provide two reasons for the quality of the shape memory behavior: the entropy of the soft segments and the modulus of the hard segments. For the EVA/PPC chains to become permanent, they need to be reheated, and thus the entropic

driving force performs the shape recovery process. The shape recovery process results from two phenomena: the entropic energy of the polymer and elastic modulus chains at low temperatures. As Fig. 10b shows about shape recovery results, the shape recovery process is better derived from higher elastic modulus values. Yan et al. [64] and Xiang et al. [65] had previously shown the importance of the elastic modulus (the temperature below and above the trigger temperature) and found that the higher the elastic modulus, the higher the shape recovery efficiency. As shown in Fig. 10b; Table 3, the shape recovery value and



elastic modulus of EVA/PP-g-MA/PPC nanocomposites (at a fixed nanofiller content) in the rubbery and glassy regions increased from GOnp to rGOnp and rGOnp/GOnp, respectively, and this increase is also greatly enhanced by increasing the nanofiller content. The simultaneous use of two nanofillers has increased the stiffness and elasticity of nanocomposites; thus, this synergic effect has developed to shape the recovery process. Since the mechanical property is excellent, the energy storage in the temporary state will be greater, and therefore the shape recovery in hybrid rGOnp/GOnp and simple GOnp and rGOnp nanocomposites will be greater. As a result, the most appropriate shape memory features are compatible with rGOnp/GOnp (1.3 phr), which contains 97.8% shape recovery and 99.3% shape fixity. In the similar work, Panahi-Sarmad et al. [46], used GO, rGO and noncovalent-fractionalized graphene with (polyamine-anchored)-perylene-bisimide (XGO) in an elastomer composite and studied its shape memory properties. They found that the shape memory recovery could increase from 86.2 to 93.4%, however, in the present study the shape recovery increased more efficiently (up to 99.3%).

## Conclusions

This research was dedicated to the study of the properties of heat-stimulated shape memory of rGOnp, GOnp, and hybrid rGOnp/GOnp incorporating EVA/PP-g-MA/PPC nanocomposites. Experimental results obtained by various tests showed that nanofillers added to EVA/PP-G-MA/PPC were arranged both in hard and soft regions. The modulus and breaking stress of prepared nanocomposites were higher than the modulus and breaking stress of the EVA/PPC blend, and the highest properties were obtained for a hybrid nanocomposite containing 1.3 phr rGOnp/GOnp. The shape memory properties are largely a function of the three parameters of nanofiller content, crystallinity, and nanofiller localization. It was found that a strong correlation between microstructure and final properties of EVA/PPC blend and nanocomposite samples can be confirmed by their thermo-mechanical behavior in three different nanofiller states. In (rGOnp/GOnp)/EVA/PP-g-MA/PPC nanocomposite shape recovery and fixity could reach 97%. The strong dependence of the phase separation to GOnp as a function nanofiller content could be observed. A very amazing improvement in the heat properties of the samples showed that the distribution of nanoparticles in the matrix was very good, which indicates the synergy effect of rGOnp and GOnp. In this research, we were able to reconcile the mechanical and shape properties of EVA/PP-g-MA/PPC nanocomposites simply by controlling the microstructure. Finally, the best shape memory specifications for hybrid nanocomposites were obtained: 98.7% shape fixity and 95.9% shape recovery.

**Supplementary Information** The online version contains supplementary material available at <https://doi.org/10.1007/s10965-024-03996-4>.

**Acknowledgements** The gratefully acknowledge the Saze Paidar Elahieh (Linkran Industrial Group) Company. The authors also thank Saze Paidar Elahie (Linkran Industrial Group), Consulting rubber Engineers CO for supporting this research.

## Declarations

**Competing interests** The authors declare that there is no conflict of interest regarding the publication of this research paper.

## References

- Jangjou A, Zareshahrabadi Z, Abbasi M, Talaiekhosani A, He Kamyab, Chelliapan S, Vaez A, Golchin A, Tayebi L, Vafa E, Amani AM, Faramarzi H (2022) Time to conquer fungal infectious diseases: employing nanoparticles as powerful and versatile antifungal nanosystems against a wide variety of fungal species. *Sustainability* 14:12942
- Hoseinzadeh A, Ghodduzi Johari H, Anbardar MH, Tayebi L, Vafa E, Abbasi M, Vaez A, Golchin A, Amani AM, Jangjou A (2022) Effective treatment of intractable diseases using nanoparticles to interfere with vascular supply and angiogenic process. *Eur J Med Res* 27:232
- Vafa E, Tayebi L, Abbasi M, Azizli MJ, Bazargan-Lari R, Talaiekhosani A, Zareshahrabadi Z, Vaez A, Amani AM, Kamyab H, Chelliapan S (2023) A better roadmap for designing novel bioactive glasses: effective approaches for the development of innovative revolutionary bioglasses for future biomedical applications. *Environ Sci Pollut Res Int*. <https://doi.org/10.1007/s11356-022-24176-1>
- Hosseinzadeh A, Zamani A, Ghodduzi Johari H, Vaez A, Golchin A, Tayebi L, Vafa E, Abbasi M, Amani AM, Chelliapan S, Kamyab H, Anbardar MH, Jangjou A (2023) Moving beyond nanotechnology to uncover a glimmer of hope in diabetes medicine: effective nanoparticle-based therapeutic strategies for the management and treatment of diabetic foot ulcers. *Cell Biochem Func* 41:517–541
- Vafa E, Azizli MJ, Tayebi L, Amani AM, Kamyab H (2024) Integrating bioactive glass with compatibilizer: a novel approach for hard tissue regeneration using PXDDA-co-PLA/PLCL/PGLA nanocomposites. *Mater Chem Phys* 316:129070
- Heidari F, Tabatabaei FS, Razavi M, Bazargan Lari R, Tavangar M, Romanos GE, Vashae D, Tayebi L (2020) 3D construct of hydroxyapatite/zinc oxide/palladium nanocomposite scaffold for bone tissue engineering. *J Mater Sci Mater Med* 31:85
- Pfau MR, Beltran FO, Woodard LN, Dobson LK, Gasson SB, Robbins AB, Lawson ZT, Saunders WB, Moreno MR, Grunlan MA (2021) Evaluation of a self-fitting, shape memory polymer scaffold in a rabbit calvarial defect model. *Acta Biomater* 136:233–242
- Heidari F, Bazargan-Lari R, Razavi M, Fahimipour F, Vashae D, Tayebi L (2020) Nano-hydroxyapatite and nano-hydroxyapatite/zinc oxide scaffold for bone tissue engineering application. *Int J Appl Ceramic Technol* 17:2752–2761
- Liu Y, Du H, Liu L, Leng J (2014) Shape memory polymers and their composites in aerospace applications: a review. *Smart Mater Struct* 23:023001
- Vafa E (2021) Bazargan-Lari R (2021) Bovine serum albumin protected gold nanozymes as a novel anti-cancer nanodrug for acute T-type lymphoblastic leukemia treatment via effect on the expression of anti-apoptotic genes. *Appl Biol Chem* 64:86

11. Mokhtary M, Najafzadeh F (2012) Polyvinylpyrrolidone-supported boron trifluoride; highly efficient catalyst for the synthesis of *N-tert*-butyl amides. *J Chem* 9:576–582
12. Gheisari F, Kasaei SR, Mohamadian P, Chelliapan S, Gholizadeh R, Zareshahabadi Z, Solhjoo SP, Vafa E, Mosleh-Shirazi S, Amani AM, Kamyab H (2024) Bromelain-loaded silver nanoparticles: formulation, characterization and biological activity. *Inorg Chem Commun* 161:112006
13. Sherif HA, Almufadi FA (2018) Analysis of elastic and plastic impact models. *Wear* 412:127–135
14. Amani AM, Tayebi L, Vafa E, Abbasi M, Vaez A, Kamyab H, Chelliapan S, Azizli MJ, Bazargan-Lari R (2024) On the horizon of greener pathways to travel into a greener future portal: green MXenes, environment-friendly synthesis, and their innovative applications. *J Clean Prod* 436:140606
15. Amani AM, Tayebi L, Abbasi M, Vaez A, Kamyab H, Chelliapan S, Vafa E (2024) The need for smart materials in an expanding smart world: MXene-based wearable electronics and their advantageous applications. *ACS Omega* 9:3123–3142
16. Mather PT, Luo X, Rousseau IA (2009) Shape Memory Polym Res 39:445–471
17. Mostafapoor F et al (2020) Interface analysis of compatibilized polymer blends. *Compatibilization of Polymer Blends*, Elsevier, pp 349–371
18. Wang L, Zhang F, Liu Y, Leng J (2022) Shape memory polymer fibers: materials, structures, and applications. *Adv Fiber Mater* 4:5–23
19. Madbouly SA, Lendlein A (2009) "Shape-memory polymer composites." *Shape-Memory Polymers*, pp 41–95
20. Chatterjee T, Dey P, Nando GB, Naskar K (2015) Hemo-responsive shape memory polymer blends based on alpha olefin and ethylene propylene diene rubber. *Polymer* 78:180–192
21. Shi G, Huang C, Cao X, Liu M, Zhang J, Zheng K, Ma Y (2021) Triple shape memory effect of ethylene-vinyl acetate copolymer/poly(propylene carbonate) blends with broad composite ratios and phase morphologies. *Polymer* 231:124144
22. Panahi-Sarmad M, Goodarzi V, Amirkiai A, Noroozi M, Abrisham M, Dehghan P, Shakeri Y, Karimpour-Motlagh N, Poudineh Hajipour F, Khonakdar HA, Asefnejad A (2019) Rograming polyurethane with systematic presence of graphene-oxide (GO) and reduced graphene-oxide (rGO) platelets for adjusting of heat-actuated shape memory properties. *Eur Polym J* 118:619–632
23. Han S, Chun BC (2014) Preparation of polyurethane nanocomposites via covalent incorporation of functionalized graphene and its shape memory effect. *Compos Appl Sci Manuf* 58:65–72
24. Tan L, Gan L, Hu J, Zhu Y, Han J (2015) Functional shape memory composite nanofibers with graphene oxide filler. *Compos A Appl Sci Manuf* 76:115–123
25. Zhang X, Xiang D, Zhu W, Zheng Y, Harkin-Jones E, Wang P, Zhao C, Li H, Wang B, Li Y (2020) Flexible and high-performance piezoresistive strain sensors based on carbon nanoparticles@polyurethane sponges. *Compos Sci Technol* 200:108437
26. Zhang H, Wang D, Wu N, Li C, Zhu C, Zhao N, Xu J (2020) Recyclable, self-healing, thermadapt triple-shape memory polymers based on dual dynamic bonds. *ACS Appl Mater Interfaces* 12:9833–9841
27. Wang W, Liu D, Liu Y, Leng J, Bhattacharyya D (2015) Electrical actuation properties of reduced graphene oxide paper/epoxy-based shape memory composites. *Compos Sci Technol* 106:20–24
28. Pirhaji A, Jebellat E, Roudbarian N, Mohammadi K, Movahhedy MR, Asle Zaem M (2022) Large deformation of shape-memory polymer-based lattice metamaterials. *Int J Mech Sci* 232:107593
29. Ebara M (2015) Shape-memory surfaces for cell mechanobiology. *Sci Technol Adv Mater* 16:014804
30. Hosoda H, Takeuchi S, Inamura T, Wakashima K (2004) Material design and shape memory properties of smart composites composed of polymer and ferromagnetic shape memory alloy particles. *Sci Technol Adv Mater* 5:503–509
31. Cambre JN, Wisian-Neilson P (2006) Poly(methylphenylphosphazene)-graft-poly(methyl methacrylate) copolymers via atom transfer radical polymerization. *J Inorg Organomet Polym Mater* 16:311–318
32. Anbarasan R, Meenarathi B, Parthasarathy V (2021) Structural and thermal studies of fluorescein and rhodamin6G grafted diblock copolymers. *J Inorg Organomet Polym Mater* 31:3549–3561
33. Roudbarian N, Baniasadi M, Ansari M, Baghani M (2019) An experimental investigation on structural design of shape memory polymers. *Smart Mater Struct* 28:095017
34. Wang X, Lu H, Liu X, Hossain M, Fu YQ, Xu BB (2020) Dynamic coordination of miscible polymer blends towards highly designable shape memory effect. *Polymer* 208:122946
35. Karasu F, Weder C (2021) Blends of poly (ester urethane) s and polyesters as a general design approach for triple-shape memory polymers. *J Appl Polym Sci* 138:49935
36. Bönisch M, Calin M, Waitz T, Panigrahi A, Zehetbauer M, Gebert A, Skrotzki W (2013) Thermal stability and phase transformations of martensitic Ti–Nb alloys. *J Eckert Sc Technol Adv Mater* 14:055004
37. El-Bayoumi A (2020) Influence of the gamma radiation on the structure of PVDF/PANI blend. *J Inorg Organomet Polym Mater* 30:613–621
38. Shao Y, Yang ZX, Deng BW, Yin B, Yang MB (2018) Tuning PVDF/PS/HDPE polymer blends to tri-continuous morphology by grafted copolymers as the compatibilizers. *Polymer* 140:188–197
39. Yang ZX, Chen Y, Liu X, Yin B, Yang MB (2020) Fabrication of poly (*ε*-caprolactone)(PCL)/poly (propylene carbonate)(PPC)/ethylene- $\alpha$ -octene block copolymer (OBC) triple shape memory blends with cycling performance by constructing a co-continuous phase morphology. *Polym Int* 69:702–711
40. Azizli MJ, Ghadami A, Vafa E, Rezaeeparto K, Parham S, Mokhtary M, Jahankhah Z, Azizli F, Bazargan-Lari R, Amani AM (2023) Compatibilization of immiscible PA6/PLA nanocomposites using graphene oxide and PTW compatibilizer for high thermal and mechanical applications. *J Polym Environ* 31:4193–4209
41. Ji S, Wang J, Olah A, Baer E (2017) Triple-shape-memory polymer films created by forced-assembly multilayer coextrusion. *J Appl Polym Sci* 134:44405
42. Jung YC, Kim JH, Hayashi T, Kim YA, Endo M, Terrones M (2012) Fabrication of transparent, tough, and conductive shape-memory polyurethane films by incorporating a small amount of high-quality graphene. *Macromol Rapid Commun* 33:628–634
43. Choi JT, Dao TD, Oh KM, Lee HI, Jeong HM, Kim BK (2012) Shape memory polyurethane nanocomposites with functionalized graphene. *Smart Mater Struct* 21:075017
44. Chen Q, Xiang D, Wang L, Tang Y, Harkin-Jones E, Zhao C, Li Y (2018) Facile fabrication and performance of robust polymer/carbon nanotube coated spandex fibers for strain sensing. *Compos Appl Sci Manuf* 112:186–196
45. Chen J, Yao B, Li C, Shi G (2013) An improved hummers method for eco-friendly synthesis of graphene oxid. *Carbon* 64:225–229
46. Panahi-Sarmad M, Abrisham M, Noroozi M, Goodarzi V, Arjmand M, Sadri M, Dehghan P, Amirkiai A, Khonakdar HA (2020) Programming polyurethane with rational surface-modified graphene platelets for shape memory actuators and dielectric elastomer generators. *Eur Polym J* 133:109745
47. Panahi-Sarmad M, Razzaghi-Kashani M (2018) Actuation behavior of PDMS dielectric elastomer composites containing optimized graphene oxide. *Smart Mater Struct* 27:085021
48. Chen J, Liu L, Liu Y, Leng J (2014) Thermoviscoelastic shape memory behavior for epoxy-shape memory polymer. *Smart Mater Struct* 23:055025

49. Joy A, Unnikrishnan G, Megha M, Haris M, Thomas J, Kolanthai E, Muthuswamy S (2022) Polycaprolactone/graphene oxide–silver nanocomposite: a multifunctional agent for biomedical applications. *J Inorg Organomet Polyme Mater* 32:912–930
50. Dreyer DR, Todd AD, Bielawski CW (2014) Harnessing the chemistry of graphene oxide. *Chem Soc Rev* 43:5288–5301
51. Chen H, Müller MB, Gilmore KJ, Wallace GG, Li D (2008) Mechanically strong, electrically conductive, and biocompatible graphene paper. *Adv Mater* 20:3557–5361
52. Azizli MJ, Abbasizadeh S, Hoseini M, Rezaeinia S, Azizli E (2017) Influence of blend composition and organic cloisite 15A content in the structure of isobutylene–isoprene rubber/ethylene propylene diene monomer composites for investigation of morphology and mechanical properties. *J Compos Mater* 51:1861–1873
53. Azizli MJ, Barghamadi M, Rezaeeparto K, Mokhtary M, Parham S (2020) Compatibility, mechanical and rheological properties of hybrid rubber NR/EPDM-g-MA/EPDM/graphene oxide nanocomposites: theoretical and experimental analyses. *Compos Commun* 22:100442
54. Azizli MJ, Barghamadi M, Rezaeeparto K, Mokhtary M, Parham S, Khademeh Molavi F, Soltani S (2021) Localization of different types of organoclay montmorillonite in the compatibilized polyamide 6/carboxylated acrylonitrile butadiene rubber nanocomposites: morphology and rheological properties. *J Appl Polym Sci* 138:51361
55. Azizli MJ, Barghamadi M, Rezaeeparto K, Mokhtary M, Parham S, Goodarzi V, Soltani S (2021) Enhancement of thermal, morphological, and mechanical properties of compatibilized based on PA6-enriched graphene oxide/EPDM-g-MA/CR: graphene oxide and EPDM-g-MA compatibilizer role. *J Appl Polym Sci* 138:49901
56. Azizli MJ, Barghamadi M, Rezaeeparto K, Mokhtary M, Parham S (2021) Graphene oxide and graphene hybrid nanocomposites based on compatibilized PP/PTW/EVA: effect of nanofiller and compatibilizer on the modeling of viscoplastic behavior. *J Polym Res* 28:1–21
57. Azizli MJ, Vafa E, Rezaeeparto K, Parham S, Mokhtary M, Jahankhah Z (2023) Preparation, characterization, and compatibilization of novel rubber nanocomposites for mechanical applications: relationship between electrical properties, morphology, and rheology. *J Adhes Sci Technol* 37:2754–2778
58. Shi Y, Chen Z (2018) Function-driven design of stimuli-responsive polymer composites: recent progress and challenges. *J Mater Chem C* 6:11817–11832
59. Strankowski M (2018) Effect of variation of hard segment content and graphene-based nanofiller concentration on morphological, thermal, and mechanical properties of polyurethane nanocomposites. *Int J Polym Sci*. <https://doi.org/10.1155/2018/1090753>
60. Azizli MJ, Barghamadi M, Rezaeeparto K, Mokhtary M, Parham S, Darabi MJ (2021) Theoretical and experimental analyses of rheological, compatibility and mechanical properties of PVMQ/XNBR-g GMA/XNBR/GO ternary hybrid nanocomposites. *Iran Polym J* 30:1001–1081
61. Jyotishkumar P, Pionteck J, Hassler RD, George SM, Cvelbar U, Thomas S (2011) Studies on stress relaxation and thermomechanical properties of poly (acrylonitrile-butadiene-styrene) modified epoxy-amine systems. *Ind Eng Chem Res* 50:4432
62. Imbernon L, Norvez S, Leibler L (2016) Stress relaxation and self-adhesion of rubbers with exchangeable links. *Macromolecules* 49:2172–2178
63. Azizli MJ, Vafa E, Rezaeeparto K, Honarkar H, Parham S, Azizli F, Tayebi L, Amani AM, Mokhtary M (2023) Impact on summation of reduced graphene oxide and compatibilization efficacy of LLDPE-g-MA on mechanical, thermal, morphological, and rheological properties of LLDPE/EVA nanocomposites. *J Polym Res* 30:420
64. Yan B, Gu S, Zhang Y (2013) Polylactide-based thermoplastic shape memory polymer nanocomposites. *Eur Polym J* 49:366–378
65. Xiang D, Zhang X, Li Y, Harkin-Jones E, Zheng Y, Wang L, Zhao C, Wang P (2019) Enhanced performance of 3D printed highly elastic strain sensors of carbon nanotube/thermoplastic polyurethane nanocomposites via non-covalent interactions. *Compos Part B Eng* 176:107250

**Publisher's Note** Springer Nature remains neutral with regard to jurisdictional claims in published maps and institutional affiliations.

Springer Nature or its licensor (e.g. a society or other partner) holds exclusive rights to this article under a publishing agreement with the author(s) or other rightsholder(s); author self-archiving of the accepted manuscript version of this article is solely governed by the terms of such publishing agreement and applicable law.